Quantum and classical two-dimensional analysis of rainbow structures in the $Xe+CO_2$ rotational excitation at 0.2 eV collision energy and on a repulsive potential

J. R. Pliego, Jr. and J. P. Braga
Departamento de Química, Universidade Federal de Minas Gerais, 31270-901 Belo Horizonte, Minas Gerais, Brazil

S. D. Bosanac
R. Boskovic Institute, Zagreb, Republic of Croatia
(Received 19 December 1994)

Rotational rainbows in the collision Xe + CO_2 are analyzed using quantum and classical two-dimensional models. We discuss the effect of the single- and the multiple-collision rotational rainbows on the differential cross sections, both for the fixed transitions and varying scattering angle and for the fixed scattering angle and varying transitions. A comparision is made with the existing centrifugal sudden calculations for this system.

PACS number(s): 34.50.−s

I. INTRODUCTION

Singularities in the differential cross section of an atom-atom collision are attributed, in classical terms, to a concentration of trajectories at a given scattering angle that has initial conditions from a range of impact parameters. Although the rainbow effect in atomic collisions has been extensively studied, the atom-molecule rainbow effect has only recently received attention [1]. The rainbow effect in this case is interpreted as a concentration of trajectories that give a maximum energy transfer to the molecule. In more exact terms, this rainbow represents a zero of the Jacobian that is associated with the transformation of the coordinates from the initial to the final states, as will be discussed later in connection with the two-dimensional analysis.

In 1983, Elber and Gerber [2], working with a diatomic molecule scattered by a surface, suggested a possibility of a type of rainbow that was due to a multiple collision of the molecule with the surface. This effect of the multiple collision can also happen in an atom-molecule collision if a heavy atom collides with a molecule with a small momentum of inertia. It turns out that this is the case for the collision process

$$Xe+CO_2(j_i)\rightarrow Xe+CO_2(j_f)\ , \tag{1.1}$$

which has been studied by Buck *et al.* [3,4]. Their theoretical analysis of this rotational energy transfer was both classical and quantal in the centrifugal sudden (CS) approximation [5,6].

The justification for the use of the CS approximation in this system was mainly pragmatic since for a collision energy of 0.2 eV it is virtually impossible to perform exact three-dimensional quantal calculations. At this energy there will be 64 open channels for the CO_2 molecule, giving rise to at least 2145 three-dimensional close-coupling equations. The quotation "exact close coupled calculations are by no means tractable" in Ref. [4] is therefore a statement that is used to justify the use of the CS approximation. However, the CS approximation is not very useful for the study of the process (1.1) since in this case there will be a large transfer of angular momentum. That was another conclusion in Ref. [4]: "the CS approximation is not expected to give reliable results under conditions [that] lead to [the] multiple collision rainbow effect." Therefore a proper quantum study of this system and in particular of its multiple collision rainbow structure has not been done yet.

Instead of using an approximate method to study the above process our approach is to assume that a large angular-momentum transfer takes place mainly when the relative angular momentum $\vec{l}$ is parallel to the rotational angular momentum of the CO_2 molecule $\vec{j}$. A two-dimensional process is then defined by assuming that the condition $\vec{l}\times\vec{j}=0$ is satisfied. This model has been explored before using a classical analysis and a hard-shape potential for the diatomic molecule [7]. In this work we develop the close-coupling equations for a two-dimensional collision, neglecting the vibrations of the CO_2 molecule. This approximation is justified because it was shown that at 1.0 eV collision energy [8], vibrations contribute less than 10% to the total cross section.

Although a two-dimensional study will not give the correct intensity in the differential cross section, its main feature, such as the position of the rainbow peaks, is expected to be reproduced since a large energy transfer is involved. This was confirmed in the two-dimensional hard ellipsoid study of the He-Na_2 system [9] and it is in agreement with the three-dimensional infinite-order sudden calculations on the same system [10]. Therefore we believe that our quantum two-dimensional analysis will be more reliable than the previous calculations of the Xe-CO_2 energy transfer.

A classical two-dimensional analysis of the Xe-CO_2 scattering was also done. This will help in the understanding of the multiple-collision rainbow effect by clarifying its dynamics. Both in classical and quantum calculations the collision energy will be fixed to 0.2 eV and the initial state of the CO_2 molecule, in the classical calculations, will be equal to zero.

II. TWO-DIMENSIONAL CLOSE-COUPLING EQUATIONS

In the two-dimensional rigid rotor approximation the Schrödinger equation for the Xe-CO_2 system can be written as [9]

$$\left\{\frac{\partial^2}{\partial R^2}+\frac{1}{R^2}\frac{\partial^2}{\partial\theta^2}+\frac{1}{R}\frac{\partial}{\partial R}+k^2 +\varepsilon\frac{\partial^2}{\partial\phi^2}-U(R,\theta-\phi)\right\}\Psi(R,\theta,\phi)=0 \quad (2.1)$$

with $k^2=2\mu_{XeCO_2}E/\hbar^2$, $\varepsilon=\mu_{XeCO_2}/I_{CO_2}$, and $U(R,\theta-\phi)=2\mu_{XeCO_2}V(R,\theta-\phi)/\hbar^2$. The atom-molecule interaction potential $V(R,\theta-\phi)$ will be discussed later. The coordinates (R,θ) are the polar coordinates of the atom and ϕ is the orientation angle of the rigid rotor. Since the potential is given as a function of the scattering coordinates and the angle $\gamma=\theta-\phi$, the transformation (θ,ϕ) to (θ,γ) will be performed. By defining the function $\psi(R,\theta,\gamma)=R^{1/2}\Psi(R,\theta,\phi)$ we obtain, for Eq. (2.1),

$$\left\{\frac{\partial^2}{\partial R^2}+\frac{1}{4R^2}+\frac{1}{R^2}\frac{\partial^2}{\partial\theta^2}+\frac{2}{R^2}\frac{\partial^2}{\partial\theta\partial\gamma} +\frac{1}{R^2}\frac{\partial}{\partial\gamma^2}+k^2+\varepsilon\frac{\partial^2}{\partial\gamma^2}-U(R,\gamma)\right\}\psi(R,\theta,\gamma)=0 . \quad (2.2)$$

This equation can be further simplified by noting that in the two-dimensional case the total angular momentum $\vec{J}$ is given as the (algebraic) sum of the internal $\vec{j}$ and the orbital $\vec{l}$ angular momenta. The elimination of the orbital angular momentum can be achieved by expanding the wave function in the eigenfunctions of the total and the internal angular momenta

$$\psi(R,\theta,\gamma)=\frac{1}{2\pi}\sum_{J,j}e^{i(J\theta-j\gamma)}\varphi_{J,j}(R) . \quad (2.3)$$

Multiplying the left-hand side of Eq. (2.2) by the complex conjugate of the above wave function and integrating over the angles we obtain

$$\left\{\frac{\partial^2}{\partial R^2}+\frac{1}{R^2}[(J-j)^2-\tfrac{1}{4}]-\varepsilon j^2+k^2\right\}\varphi_{J,j}(R) -\sum_{J',j'}U_{Jj,J'j'}(R)\varphi_{J',j'}(R)=0 \quad (2.4)$$

with

$$U_{Jj,J'j'}=\frac{\delta_{J,J'}}{2\pi}\int_0^{2\pi}e^{i(j-j')\gamma}U(R,\gamma)d\gamma . \quad (2.5)$$

These are the two-dimensional close-coupling equations to be solved.

In the asymptotic region the solutions of the close-coupling equations are now matched to

$$\varphi_\lambda(R)=\frac{1}{R^{1/2}}[\varphi_\lambda^{(-)}(R)-S_{j,j'}\varphi_\lambda^{(+)}(R)] , \quad (2.6)$$

where $S_{j,j'}$ is an element of the scattering matrix and $\lambda=J-j$. The functions $\varphi_\lambda^{(\pm)}(R)$ are given by

$$\varphi_\lambda^{(\pm)}(R)=\left[\frac{2\pi}{\rho}\right]^{1/2}e^{\pm i(\rho-\lambda\pi/2-\pi/4)} =J_\lambda(\rho)\pm iY_\lambda(\rho) \quad (2.7)$$

for the open channels, i.e., $\rho^2=(k^2-\varepsilon j^2)R^2>0$, and

$$\varphi_\lambda^-(R)=0 , \qquad \varphi_\lambda^+(R)=\left[\frac{1}{2\pi\rho}\right]^{1/2}e^{-\rho}=K_\lambda(\rho) \quad (2.8)$$

for the closed channels, i.e., $\rho^2<0$. The functions $J_\lambda(\rho)$ and $Y_\lambda(\rho)$ are the Bessel functions of first and second order whereas $K_\lambda(\rho)$ is the modified Bessel function [11].

The scattering amplitude $f_{j,j'}(\theta)$ is now calculated by applying the boundary condition

$$\Psi=e^{i(k_jz+j\phi)}+\frac{1}{R^{1/2}}\sum_{j'}e^{i(k_{j'}z+j'\phi)}f_{j,j'}(\theta) \quad (2.9)$$

and expanding the plane waves into Bessel functions. A comparison with (2.3) gives

$$f_{j,j'}(\theta)=-\frac{e^{-i\pi/4}e^{i(j'-j)\pi/2}}{(2\pi k_{j'})^{1/2}} \times\sum_{J=-\infty}^{J=\infty}(\delta_{j,j'}-S^J_{j,j'})e^{i(J-j')\theta} , \quad (2.10)$$

from which the differential cross section can be obtained.

The close-coupling equations were solved by the log-derivative method [12]. The close-coupling equations were integrated from 2 to 10 Å with a step size equal to 0.0025 Å. In our calculations the converged results were obtained by taking partial waves from $J=-350$ to 350.

III. POTENTIAL INTEGRALS

The atom-molecule potential that we use here is the same as the one used by Buck *et al.* [3,4] and consists of a Hartree-Fock dispersion-type potential with an expansion into the Legendre functions both in the short-range and in the long-range regions. Its analytic form is

$$V(R,\gamma)=e^{\alpha[R_a(\gamma)-R]} -\sum_{l=0,2,4}\left[\frac{C_6^{(l)}}{R^6}+\frac{C_8^{(l)}}{R^8}\right]f(R)P_l(\cos\gamma) , \quad (3.1)$$

with $R_a(\gamma)=R_0[1+R_2P_2(\cos\gamma)]$, and the damping function of $f(R)$ is given by

$$f(R)=\begin{cases}e^{-(D/R-1)^2}, & R\le D\\ 1, & R>D.\end{cases} \quad (3.2)$$

The potential has an attractive part with a well depth of

33.6 meV at $R=3.83$ Å. In this paper we will consider only the repulsive part of the potential, i.e., the function $f(R)$ will be assumed to be zero everywhere. Constants for the repulsive part of this potential are given in Table I.

TABLE I. Constants to be used in the repulsive potential.

α (Å^{-1})	R_0 (Å)	R_2 (Å)	D (Å)
3.4	3.1	0.2	4.4

The calculation with only the repulsive short-range part of the potential will help us understand the multiple-collision rainbow effect and the importance of the long-range forces on this effect [13]. The calculation can also be used for testing the quality of the impulsive collision model where a short-range infinite barrier substitutes for the whole potential [14].

For the potential given in the form of the expansion in the angular functions, the integrals (2.6) can be calculated and are given by

$$\begin{aligned} U_{Jj,J'j'} &= \delta_{J,J'}\left[\frac{\mu_{XeCO_2}}{\pi\hbar^2}\right]\int_0^{2\pi} e^{i(j-j')\gamma} V(R,\gamma)\,d\gamma \\ &= \delta_{J,J'}\left[\frac{\mu_{XeCO_2}}{\pi\hbar^2}\right]\int_0^{2\pi} e^{i(j-j')\gamma} e^{\alpha\{R_0[1+R_2P_2(\cos 2\gamma)]-R\}}\,d\gamma \\ &= \delta_{J,J'}\left[\frac{\mu_{XeCO_2}}{\pi\hbar^2}\right] e^{[\alpha(R_0-R)+\alpha R_0R_2/4]}\int_0^{2\pi} e^{i(j-j')} e^{3\alpha R_0R_2\cos(2\gamma)/4}\,d\gamma\ . \end{aligned} \tag{3.3}$$

Using the symmetry property of this integral we arrive at the expressions for the matrix elements of the potential

$$\begin{aligned} U_{Jj,J'j'} &= \delta_{J,J'}\left[\frac{\mu_{XeCO_2}}{\pi\hbar^2}\right] e^{[\alpha(R_0-R)+\alpha R_0R_2/4]}\int_0^{2\pi} e^{i(j-j')\gamma} e^{3\alpha R_0R_2\cos(2\gamma)/4}\,d\gamma \\ &= \delta_{J,J'}\left[\frac{\mu_{XeCO_2}}{\pi\hbar^2}\right] e^{[\alpha(R_0-R)+\alpha R_0R_2/4]}[1+(-1)^{j-j'}]\int_0^{\pi} e^{3\alpha R_0R_2\cos(2\gamma)/4}\cos[(j-j')\gamma]\,d\gamma \end{aligned} \tag{3.4}$$

or

$$\begin{aligned} U_{Jj,J'j'} = \delta_{J,J'}&\left[\frac{2\pi\mu_{XeCO_2}}{\hbar^2}\right] e^{[\alpha(R_0-R)+\alpha R_0R_2/4]} \\ &\times\left[\frac{[1+(-1)^{j-j'}]}{4}\right] I_{(j-j')/2}(3\alpha R_0R_2/4)\ . \end{aligned} \tag{3.5}$$

The function $I_{(j-j')/2}(3\alpha R_0R_2/4)$ is the integral representation of the regular modified Bessel function and is calculated by using a representation given by the Taylor expansion of its argument [11]. The above relationship therefore gives the potential matrix that is used in the close-coupling equations.

IV. CLASSICAL TRAJECTORY

Hamilton's equations in the coordinates (R,θ,φ) were solved by the fourth-order Runge-Kutta method, from which the scattering angle and the final angular momentum were calculated. The angle φ and the impact parameter b were generated randomly in the intervals $0\le\varphi\le\pi$ and -6 Å$\le b\le 6$ Å, respectively. To achieve convergence of about 1% in the differential cross section, a total number of 200 000 trajectories was needed.

A set of trajectories that is initially in the interval $dA_i=dbd\varphi$ ends up in the interval $dA_f=d\theta dj$. If the initial and the final densities of the trajectories are ρ_i and ρ_f, respectively, we have [15]

$$\rho_f=\sum\rho_i\frac{dbd\phi}{d\theta dj}\ , \tag{4.1}$$

which gives, for the two-dimensional classical differential cross section,

$$\sigma_{j,j'}(\theta)=\frac{1}{2\pi}\sum\left|\frac{\partial(\theta,j)}{\partial(b,\phi)}\right|^{-1}\ . \tag{4.2}$$

The summation above has to be over all the initial values of (b,ϕ) that lead to the given final (θ,j').

Singularity in the cross section will then happen whenever the condition

$$g(\theta,j)=\frac{\partial(\theta,j)}{\partial(b,\phi)}=0 \tag{4.3}$$

is satisfied. For the given initial conditions Eq. (4.3) determines the rainbow position in the (j,θ) plane and consequently a rainbow trajectory in this plane.

However, as we have checked numerically in a few examples, the above condition is too restrictive and may be substituted by

$$\left[\frac{\partial j}{\partial\varphi}\right]_b\left[\frac{\partial\theta}{\partial b}\right]_\varphi=0\ , \tag{4.4}$$

a condition that has also been found before [16]. Under this approximation the rainbows are classified as the rotational (with the first term equal to zero) or of the "1" type (with the second term equal to zero). The second rainbow, which is analogous to the atom-atom rainbow, ap-

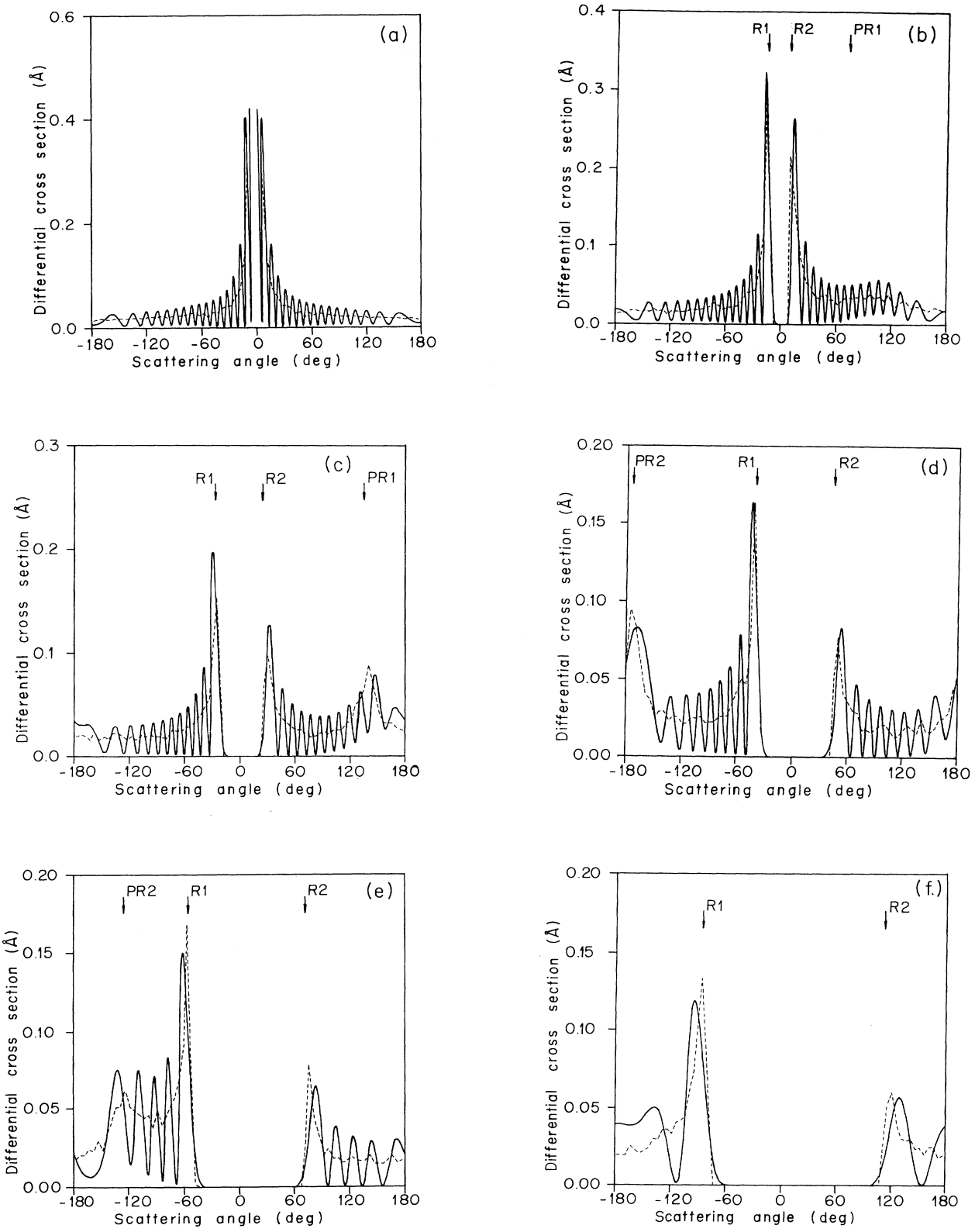

FIG. 1. (a) Differential cross section as a function of the scattering angle for the 0→0 transition. Full lines are for quantum calculations, whereas the dotted lines are for the classical calculations. (b) Same as (a) but for the 0→10 transition. (c) Same as (a) but for the 0→20 transition. (d) Same as (a) but for the 0→30 transition. (e) Same as (a) but for the 0→40 transition. (f) Same as (a) but for the 0→50 transition.

pears in our calculations at very small angles where the differential cross section is itself large. Consequently, only the rotational rainbows will be discussed here, although calculations were made using Eq. (4.3).

V. THE DIFFERENTIAL CROSS SECTION FOR THE FIXED ROTATIONAL TRANSITION

In Figs. 1(a)–1(f) we present classical and quantum differential cross sections (DCSs) as functions of the scattering angle and for fixed rotational transitions. Only the transitions to the positive rotational angular momentum will be discussed since there is an obvious symmetry in the differential cross section regarding the transformation $j \rightarrow -j$ and $\theta \rightarrow -\theta$. The agreement between the classical and the quantum calculations is clear from these figures. This is due to the nature of the problem that we solve, namely, the forces are entirely repulsive. In this case, transitions to the closed channels in the interaction region are not important. A calculation with the full potential [13] will show that this is indeed the case.

For the elastic transition the DCS is symmetric with respect to $\theta=0°$ since this is equivalent to the static limit where no transitions are allowed. As the final angular momentum is increased the rainbow structure starts to appear, as shown in Figs. 1(b)–1(f). The solutions of Eq. (4.3) were found and they are represented in these figures by the arrows R1, R2, PR1, and PR2. A discussion of these rainbows will be presented below.

We expect that j_R is proportional to θ_R, which is confirmed in Fig. 1, but it has also been predicted in the atom ellipsoid model [7]. We can therefore write

$$g(\theta,j)=j-2k(A-B)\sin(\theta/2)=0 , \tag{5.1}$$

where A and B are the principal axes of the ellipsoid. For the system that we study here we have calculated $A-B=0.926$ Å and give for the solution of the above equation

$$j_R=104,0\sin(\theta_R/2) . \tag{5.2}$$

In Table II a comparison is shown for the calculated rotational angular momentum (for some points of the R1 branch) using this equation and using the classical trajectory method. The agreement is reasonable only for the low transitions and we conclude that the classical impulsive model is not adequate for the study of the Xe-CO_2+ system at 0.2 eV collision energy. On the basis of our classical-quantum agreement, we also believe that the quantum impulsive model [9] is not appropriate to describe this system. This conclusion also applies to the other impulsive approximations such as the centrifugal sudden approximation or the infinite-order sudden approximation. Our analysis here in fact reinforces the conclusions of Buck *et al.*

TABLE II. Comparison of the rainbow angular momentum calculated from the impulsive model and the classical trajectory. Dates are relative to the R1 branch.

θ_R (deg)	j_R from the impulsive model	"Exact" classical j_R
4	4	2
10	9	6
17	15	10
23	21	14
30	27	18
34	30	20
42	37	24
61	52	32

VI. RAINBOW TRAJECTORIES

The nature of the rainbows R1, R2, PR1, and PR2 can be clarified by analyzing the Jacobian [Fig. 2(a)], the final classical rotational angular momentum [Fig. 2(b)], and the scattering angle [Fig. 2(c)], as functions of the initial orientation of the CO_2 molecule and for the head-on collision. The results of this analysis are shown in Fig. 2. In Fig. 2(b) the dotted line represents the rotational angular momentum after the first encounter, whereas the full line is for the final angular momentum.

There are four regions in Fig. 2(a) that we should be concerned with: the points where the Jacobian is zero, denoted by (1) and (4), and the region where the Jacobian is very small, denoted by (2) and (3). The points (1) and (4) will give rise to the singularity in the classical differential cross section. Its associated angular momentum and angle are therefore the j_R and θ_R, as can be seen from Figs. 2(b) and 2(c). Figure 2 confirms that these two rainbows are the rotational rainbows and that the first term in the Jacobian is the dominant one. All other rain-

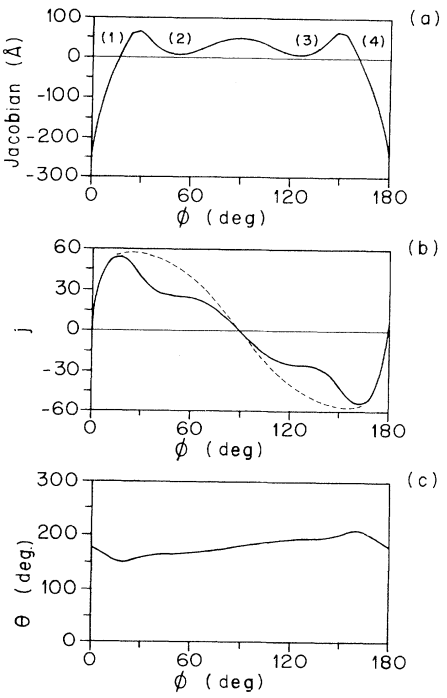

FIG. 2. Dependence of the Jacobian, the final rotational state, and the scattering angle on the orientation of the CO_2 molecule. The impact parameter is equal to zero.

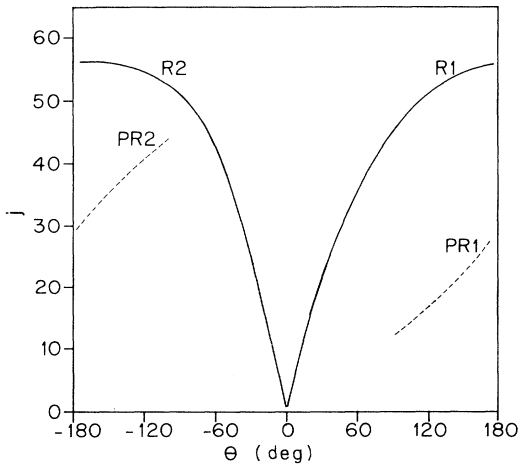

FIG. 3. Single (R1 and R2) and multiple (PR1 and PR2) rotational rainbow trajectories.

bows in this work have the same characteristic as above, i.e., they are the rotational rainbows, but the rainbow R1 and R2 are characterized by a single encounter since the final angular momentum is the same as the angular momentum in the first encounter.

The other two regions (2) and (3) are characterized by two encounters, as shown in Fig. 2(b). Since the Jacobian is very small at these points the cross section will, as a consequence, be larger compared with the neighboring points. In this sense we also call these points the rainbow points. Since they are not the rainbows for which the Jacobian is strictly zero we prefer to call them the pseudorainbows (PR). If they are of type 1 then we denote them as PR1 and if they are of type 2 then PR2. The manifestation of these pseudorainbows, which are of the multiple-collision nature, on the cross section is clear from Fig. 1, being confirmed by classical and quantum calculations. We believe that these pseudorainbows have not been reported before or they might have been misinterpreted.

We have analyzed the position of these rainbows in the j_R-θ_R plane for different impact parameters and the results are plotted in Fig. 3. Due to the symmetry discussed before, only half of the figure is presented.

The branches R1 and R2 are the rainbows predicted by the atom-ellipsoid model. An attempt to incorporate the multiple collision rainbow effect into this theory has been made [17]. The conclusion was that the single-collision rainbow disappears in the presence of the multiple-collision rainbow, resulting in a broken line, for example, from rainbow R1 to PR1. Our calculations, both quantum and classical, show that this is not the case. For a given initial condition we can have the same angular momentum for two scattering angles at the single- and the multiple-collision region.

VII. THE DIFFERENTIAL CROSS SECTION AS A FUNCTION OF THE FINAL ANGULAR MOMENTUM

At a fixed scattering angle there are two states of a given rotational angular momentum j that contribute to the differential cross section: one is $+j$ and the other is $-j$. In our analysis we add the contribution of the two and call it the state to state differential cross section. The results of one calculation of this type are shown in Fig. 4, where the rainbows R1, R2, PR1, and PR2 have also been marked.

Although calculations in Ref. [4] are in three dimensions and for the complete potential, it is interesting to compare the differential cross sections presented here with those calculated in the above reference. It should be noted, however, that the CS approximation is not able to distinguish the right-left asymmetry and therefore we expect to have more peaks in the differential cross section.

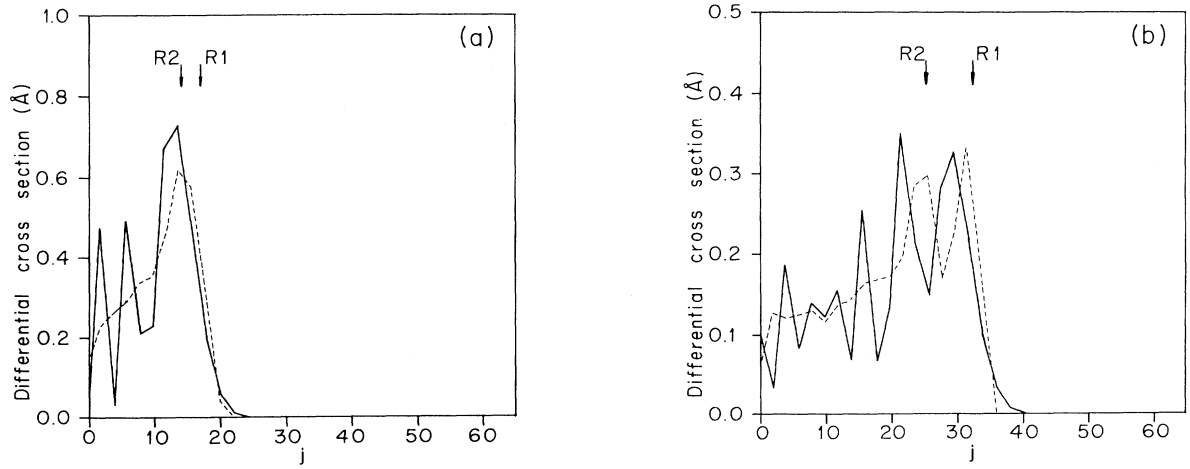

FIG. 4. (a) Differential cross section as a function of the final rotational state for $\theta=20°$. Full lines are for the quantum calculations, whereas the dotted lines are for the classical calculations. (b) Same as in (a) but for $\theta=40°$. (c) Same as in (a) but for $\theta=80°$. (d) Same as in (a) but for $\theta=120°$. (e) Same as in (a) but for $\theta=180°$.

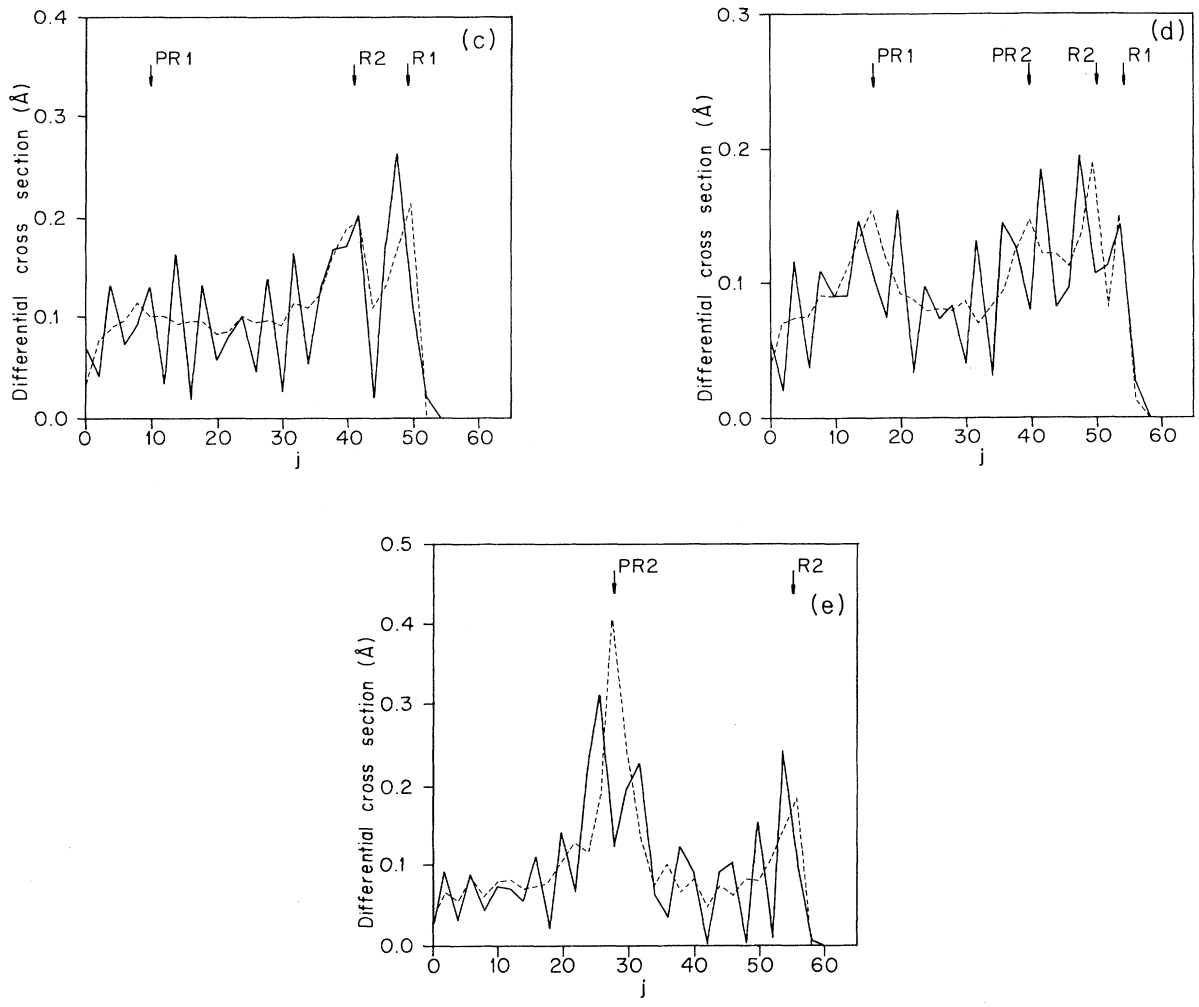

FIG. 4. (*Continued*).

The restriction to a two-dimensional analysis also implies that the magnitude of the DCS is smaller compared to the three-dimensional calculation.

Transitions into the $\theta=180°$ scattering angle are interesting to study. The CS calculation [4] predicts three peaks in the DCS: one that is a single-collision transition and has a peak at $j\cong 60$ and two that are of a multiple-collision nature and have peaks for $j\cong 14$ and 24. The present calculation shows only two peaks: one of single-collision nature at $j\cong 60$ and one of multiple-collision nature at $j\cong 28$. In fact, the calculation with the full potential [13] will show that another peak, which occurs at $j\cong 10$, will be present in the differential cross section.

The right-left asymmetry manifest itself at $\theta=120°$ where four peaks appear in the presently calculated DCS, whereas only three peaks occur in the DCS calculated in Ref. [4]. For the single-collision rainbow it is difficult to say which of the rainbows is present in the calculation reported in Ref. [4], but for the multiple-collision rainbow the situation can be clarified since these rainbows have different behavior in the $j\times\theta$ plane. Reference [4] failed to identify the rainbow denoted here by PR1, as can be confirmed from the nature of the rainbows, as presented in Fig. 3.

For the differential cross sections at $\theta=80°$ the PR2 rainbow disappears in our calculation while the results of Buck *et al.* still show this peak, but failed to identify the PR1 branch, which has moved to a small angular momentum. The occurrence of this peak at a small energy transfer is in agreement with the experimental energy-loss spectra [4].

At $\theta=40°$ and 20° the disagreements between the results are more evident and both calculations should be taken as approximate. In the present calculation this is mainly due the importance of the long range of the potential and in the case of the CS approximation because the centrifugal term becomes more important.

ACKNOWLEDGMENT

We would like to thank the Brazilian National Research Council for financial support.

[1] H. J. Korsch and A. Ernesti, J. Phys. B **25**, 3565 (1992).
[2] R. Elber and G. Gerber, J. Chem. Phys. **79**, 4087 (1983).
[3] U. Buck, F. Huisken, D. Otten, and R. Schinke, Chem. Phys. Lett. **101**, 126 (1983).
[4] U. Buck, D. Otten, R. Schinke, and D. Poppe, J. Chem. Phys. **82**, 202 (1985).
[5] R. T. Pack, J. Chem. Phys. **60**, 633 (1974).
[6] P. McGuire and D. Kouri, J. Chem. Phys. **60**, 2488 (1974).
[7] S. D. Bosanac, Phys. Rev. A **22**, 2617 (1980).
[8] G. Billing, Chem. Phys. Lett. **117**, 145 (1985).
[9] S. D. Bosanac, Phys. Rev. A **26**, 282 (1982).
[10] H. J. Korsch and R. Schinke, J. Chem. Phys. **75**, 3850 (1981).
[11] *Handbook of Mathematical Functions,* edited by M. Abramowitz and I. A. Stegun (Dover, New York, 1965).
[12] B. R. Johnson, J. Comput. Phys. **13**, 445 (1973).
[13] J. R. Pliego, Jr., J. P. Braga, and S. D. Bosanac (unpublished).
[14] S. D. Bosanac and N. Petrovic, Phys. Rev. A **41**, 5909 (1990).
[15] L. D. Thomas, Chem. Phys. Lett. **51**, 35 (1977).
[16] J. M. Bowman and K. T. Lee, J. Chem. Phys. **74**, 2664 (1981).
[17] S. D. Bosanac, Chem. Phys. Lett. **103**, 484 (1984).